NASA/CR–2013-217974
NIA Report No. 2013-0116

Analysis of an Aircraft Honeycomb Sandwich Panel with Circular Face Sheet/Core Disbond Subjected to Ground-Air Pressurization

Martin Rinker
Fraunhofer-Institut für Werkstoffmechanik IWM, Halle, Germany

Ronald Krueger and James Ratcliffe
National Institute of Aerospace, Hampton, Virginia

March 2013

NASA STI Program . . . in Profile

Since its founding, NASA has been dedicated to the advancement of aeronautics and space science. The NASA scientific and technical information (STI) program plays a key part in helping NASA maintain this important role.

The NASA STI program operates under the auspices of the Agency Chief Information Officer. It collects, organizes, provides for archiving, and disseminates NASA's STI. The NASA STI program provides access to the NASA Aeronautics and Space Database and its public interface, the NASA Technical Report Server, thus providing one of the largest collections of aeronautical and space science STI in the world. Results are published in both non-NASA channels and by NASA in the NASA STI Report Series, which includes the following report types:

- TECHNICAL PUBLICATION. Reports of completed research or a major significant phase of research that present the results of NASA Programs and include extensive data or theoretical analysis. Includes compilations of significant scientific and technical data and information deemed to be of continuing reference value. NASA counterpart of peer-reviewed formal professional papers, but having less stringent limitations on manuscript length and extent of graphic presentations.

- TECHNICAL MEMORANDUM. Scientific and technical findings that are preliminary or of specialized interest, e.g., quick release reports, working papers, and bibliographies that contain minimal annotation. Does not contain extensive analysis.

- CONTRACTOR REPORT. Scientific and technical findings by NASA-sponsored contractors and grantees.

- CONFERENCE PUBLICATION. Collected papers from scientific and technical conferences, symposia, seminars, or other meetings sponsored or co-sponsored by NASA.

- SPECIAL PUBLICATION. Scientific, technical, or historical information from NASA programs, projects, and missions, often concerned with subjects having substantial public interest.

- TECHNICAL TRANSLATION. English-language translations of foreign scientific and technical material pertinent to NASA's mission.

Specialized services also include organizing and publishing research results, distributing specialized research announcements and feeds, providing information desk and personal search support, and enabling data exchange services.

For more information about the NASA STI program, see the following:

- Access the NASA STI program home page at *http://www.sti.nasa.gov*

- E-mail your question to help@sti.nasa.gov

- Fax your question to the NASA STI Information Desk at 443-757-5803

- Phone the NASA STI Information Desk at 443-757-5802

- Write to:
  STI Information Desk
  NASA Center for AeroSpace Information
  7115 Standard Drive
  Hanover, MD 21076-1320

NASA/CR–2013-217974
NIA Report No. 2013-0116

Analysis of an Aircraft Honeycomb Sandwich Panel with Circular Face Sheet/Core Disbond Subjected to Ground-Air Pressurization

Martin Rinker
Fraunhofer-Institut fürWerkstoffmechanik IWM, Halle, Germany

Ronald Krueger and James Ratcliffe
National Institute of Aerospace, Hampton, Virginia

National Aeronautics and
Space Administration

Langley Research Center
Hampton, Virginia 23681-2199

Prepared for Langley Research Center
under Cooperative Agreement NNL09AA00A

March 2013

Available from:

NASA Center for AeroSpace Information
7115 Standard Drive
Hanover, MD 21076-1320
443-757-5802

Analysis of an Aircraft Honeycomb Sandwich Panel with Circular Face Sheet/Core Disbond Subjected to Ground-Air Pressurization

Martin Rinker[*], Ronald Krueger[†] and James Ratcliffe[†]

Abstract

The ground-air pressurization of lightweight honeycomb sandwich structures caused by alternating pressure differences between the enclosed air within the honeycomb core and the ambient environment is a well-known and controllable loading condition of aerospace structures. However, initial face sheet/core disbonds intensify the face sheet peeling effect of the internal pressure load significantly and can decrease the reliability of the sandwich structure drastically. Within this paper, a numerical parameter study was carried out to investigate the criticality of initial disbonds in honeycomb sandwich structures under ground-air pressurization. A fracture mechanics approach was used to evaluate the loading at the disbond front. In this case, the strain energy release rate was computed via the Virtual Crack Closure Technique. Special attention was paid to the pressure-deformation coupling which can decrease the pressure load within the disbonded sandwich section significantly when the structure is highly deformed. The commercial finite element analysis software, ABAQUS®/Standard, was used for the analyses and the recursive pressure-deformation coupling was solved by applying fluid cavities. The results show that disbond size, face sheet thickness and core thickness are important parameters that determine crack tip loading at the disbond front. Further, the pressure-deformation coupling was found to have an important load decreasing effect. Without considering the observed pressure drop in the bulged sandwich, the loading at the disbond front would be significantly higher and the initial disbond would be even more critical.

Nomenclature

a_P	Panel length
b_P	Panel width
h_c	Core thickness
h_f	Face sheet thickness
r_{disb}	Disbond radius
a_{disb}	Disbond length
b_{disb}	Disbond width
H	Elevation or altitude above mean sea level

[*] Fraunhofer Institute for Mechanics of Materials IWM, Walter-Huelse-Strasse 1, 06120 Halle, Germany.

[†] National Institute of Aerospace, 100 Exploration Way, Hampton, VA, 23666, resident at Durability, Damage Tolerance and Reliability Branch, MS 188E, NASA Langley Research Center, Hampton, VA, 23681, USA.

H_0	Ground elevation above mean sea level of the launch site or airport
H_1	Operating altitude above mean sea level during flight
p	Pressure
$p_{a,0}$	Ambient pressure at H = H_0 according to ISO Standard Atmosphere
$p_{disb,0}$	Pressure in the disbonded sandwich section at H = H_0
$p_{int,0}$	Pressure in the intact sandwich section at H = H_0
$p_{a,1}$	Ambient pressure at H = H_1 according to ISO Standard Atmosphere
$p_{disb,1}$	Pressure in the disbonded sandwich section at H = H_1
$p_{int,1}$	Pressure in the intact sandwich section at H = H_1
T	Temperature
$T_{a,0}$	Ambient temperature at H = H_0 according to ISO Standard Atmosphere
$T_{disb,0}$	Temperature in the disbonded sandwich section at H = H_0
$T_{int,0}$	Temperature in the intact sandwich section at H = H_0
$T_{a,1}$	Ambient temperature at H = H_1 according to ISO Standard Atmosphere
$T_{disb,1}$	Temperature in the disbonded sandwich section at H = H_1
$T_{int,1}$	Temperature in the intact sandwich section at H = H_1
V	Volume
$V_{disb,0}$	Volume of the disbonded sandwich section at H = H_0
$V_{int,0}$	Volume of the intact sandwich section at H = H_0
$V_{disb,1}$	Volume of the disbonded sandwich section at H = H_1
$V_{int,1}$	Volume of the intact sandwich section at H = H_1
R	Universal gas constant
n	Amount of substance
E_{11}	Young's modulus along the x-axis of the orthotropic material coordinate system
E_{22}	Young's modulus along the y-axis of the orthotropic material coordinate system
E_{33}	Young's modulus along the z-axis of the orthotropic material coordinate system
v_{12}	Poisson's ratio in the x-y-plane of the orthotropic material coordinate system
v_{13}	Poisson's ratio in the x-z-plane of the orthotropic material coordinate system
v_{23}	Poisson's ratio in the y-z-plane of the orthotropic material coordinate system
G_{12}	Shear modulus in the x-y-plane of the orthotropic material coordinate system
G_{13}	Shear modulus in the x-z-plane of the orthotropic material coordinate system
G_{23}	Shear modulus in the y-z-plane of the orthotropic material coordinate system
G_I	Mode I strain energy release rate
G_{II}	Mode II strain energy release rate
G_{III}	Mode III strain energy release rate
G_T	Total strain energy release rate ($G_I + G_{II} + G_{III}$)
G_c	Fracture toughness

1. Introduction

Honeycomb sandwich structures exhibit high stiffness and strength-to-weight ratios and therefore are widely used as structural components, especially within the aerospace industry [1, 2]. Sandwich structures become most effective with low density and thick cores. The volume of these light-weight honeycomb core materials typically consist of up to 95% enclosed air. If the sandwich structure is subjected to varying ambient pressure, temperature and/or humidity, and if airflow into and out of the sandwich core is prohibited, the resulting pressure difference causes mechanical stress. During the ascent of aircraft and the launch of space systems, their honeycomb sandwich structures are subjected to tensile stress in the core, and in the bondline between face sheet and core, caused by the decreasing ambient pressure. The focus of the current investigation is for aircraft honeycomb structures. However, the first problems related to internal pressurization arose in space systems. Since their use in the early 1960's, several honeycomb sandwich structures of space systems have failed during launch due to face sheet/core disbonding [3, 4]. A major recommendation that arose from the subsequent accident investigations was the use of fully vented sandwich constructions for space systems. This means that the sandwich should not only be vented between each core cell but also through the face sheets. If the use of a vented design is not possible, the structural integrity should be verified via in-flight condition testing and non-destructive testing of the face sheet/core bond [4]. However, large-scale face sheet/core disbonding in unvented sandwich construction occurred again in the liquid hydrogen tank of the X-33 technology flight demonstration vehicle during the protoflight test in 1999 [5, 6]. The internal pressurization of the core was caused by *cryopumping,* which can create much higher loads than the atmospheric pressure. This structural failure was cited as a major reason to stop the *VentureStar* suborbital spaceplane program.

Because of their lower operating altitude, aircraft honeycomb sandwich structures experience lower loads during flight compared to space systems. Often, the use of fully vented sandwich constructions is not possible. Although intact honeycomb sandwich structures have been widely used in aircrafts for many years, face sheet/core disbonding can be critical when the bondline between face sheet and core is weak or damaged due to impacts or inadequate repairs. In the last decades, face sheet/core disbonding in honeycomb sandwich structures have occurred in large passenger aircrafts [7, 8, 9, 10, 11]. Among initial disbonds, or weak face sheet/core interfaces, internal pressurization was another major cause of the disbond propagation. In another example, the loss of a rudder on a commercial aircraft was found to be due to disbonding within the sandwich structure of the rudder, growth of which was driven by internal pressurization at flight altitude [10, 11]. A key conclusion of these incidents is that critical face sheet disbond size and the parameters affecting disbond growth become very

important for the damage tolerance evaluation of an aircraft sandwich component during its design phase and in service.

In the current paper, the results of a numerical study are presented where a pressurized honeycomb sandwich panel containing a circular disbond between face sheet and core was modeled. A fracture mechanics approach was used and the Virtual Crack Closure Technique was applied to calculate the energy release rate along the disbond front, an approach that is widely used for the analysis of delaminations in monolithic composites [12, 13]. Due to the presence of oscillatory terms in the stress and strain fields at the crack front of a bi-material interface (such as a face sheet/core disbond), mode I and mode II energy release rate components are not well defined. Therefore, only the total energy release rate G_T, which does have a definite converged value [14,15], was considered in the current study.

Due to the enclosed air, the structural analysis becomes a recursive problem. Since the ideal gas law has to be considered, not only the deformation behavior of the sandwich depends on the applied pressure load, but the applied pressure also depends on the volume change and on the deformation. Therefore, a non-linear finite element analysis was performed for coupling the ideal gas law for the air filled cavity with the deformation analysis of the sandwich. The aim of this work was to investigate the influence of the most important sandwich parameters on the criticality of internally pressurized, partially disbonded, honeycomb sandwich structures. A generic flat sandwich panel was modeled containing circular face sheet/core disbonds with radii ranging from 50.8 mm (2") to 762 mm (30"), face sheet thicknesses from 0.772 to 5.404 mm (from 0.03" to 0.21"), core thicknesses from 12.7 to 76.2 mm (from 0.5" to 3") and core densities from 29 to 80 kg/m^3 (1.8 to 5.0 lb/ft^3).

2. Problem description

A flat sandwich panel, consisting of laminated composite face sheets and a honeycomb core with an initial circular disbond at the upper face sheet/core interface, was considered as shown in Figure 1. It is assumed that the sandwich panel is much larger than the disbonded section, which is completely surrounded by the intact part. The honeycomb core is assumed to be unvented. Consequently, air flow and rapid pressure equalization inside the sandwich can only occur between the honeycomb cells in the disbonded section. Air flow and rapid pressure equalization with the environment is prevented. However, due to permeability, slow pressure equalization can also occur between the cell walls of the intact section and through the composite face sheets between the sandwich core and the environment [5, 16]. For this reason, the pressure is initially assumed equal inside and outside the sandwich ($p_{a,0} = p(H_0) = p_{disb,0}$) and thus the sandwich structure is not loaded (Figure 1(a)).

When the ambient pressure decreases rapidly, for instance during the launch of a spacecraft or the ascent of an aircraft, pressure equalization due to permeability becomes significant. The resulting pressure difference $\Delta p = p_{disb,1} - p_{a,1}$ expands the sandwich. In the disbonded section the thin face sheets with low bending stiffness (which is normally ideal for optimizing the sandwich effect) can easily be deformed by the out of plane pressure load and bulge the sandwich as shown in Figure 1(b). This results in an increased volume, *V*, and lower pressure, *p*, which can be calculated using the ideal gas law

$$pV = nRT \tag{1}$$

In Equation 1, *T* is the temperature of the gas, *R* = 8.314 J/(mol K) is the universal gas constant and *n* is the amount of substance of gas (also known as number of moles). In this case the gas is the enclosed air. It is obvious that the pressure in the sandwich core additionally decreases with decreasing temperature at higher flight altitudes, H. Bulging is prevented in the intact section by the honeycomb cell walls. Hence, volume increase is only possible due to out of plane deformation of the core. Thus, the pressure change in the intact section is dominated mainly by the temperature change and can easily be calculated by Eq. 1. If significant bulging occurs in the disbonded section, the resulting recursive pressure-deformation problem needs to be solved.

3. Finite Element Modeling

ABAQUS®/Standard[1] and ABAQUS®/CAE scripting interface (Version 6.12) were used for the three-dimensional finite element analysis and the parameterized pre- and post-processing, respectively. A typical finite element model of the panel is shown in Figure 2. With symmetry conditions at two planes perpendicular to one another with respect to the disbond center only a quarter-model was used. The overall panel dimensions depended directly on the disbond radius, r_{disb}. The panel length a_P and width b_P were always four times as large as r_{disb}. In the presented study, the disbond radius ranged from 50.8 mm (2”) to 762 mm (30”). ABAQUS®/Standard 20-node quadratic brick elements (C3D20) having orthotropic and laminate properties were used for the honeycomb core and the face sheets [17]. For modeling purposes, the core was assumed to be a homogeneous, orthotropic material. The mesoscopic honeycomb cell structure is not considered in order to keep the model simple. Since the major interest of the calculations focused on the disbonded sandwich section and the vicinity of the crack front, a fine mesh was used for the circular disbonded part (particularly the crack front). An element length, Δa=1.0 mm, was used for the elements surrounding the crack front as shown in the

[1] ABAQUS® is a product of Dassault Systèmes Simulia Corp. (DSS), Providence, RI, USA

enlarged detail in Figure 2. This area of detail was surrounded by a coarse mesh for the square intact part. Surface based contact was used to prevent the penetration of the disbonded sandwich parts. The investigated sandwich is symmetric with respect to the mid-plane. Consequently, both face sheets consist of the same material lay-up and have the same thickness, h_f. CYCOM®[2] 5320 plain weave fabric with a quasi-isotropic [45/0/90/-45] stacking sequence was used as face sheet material. For the current investigations, this four-ply stack with an overall thickness of 0.772 mm (0.03") served as the basic unit. This stack was then repeated up to seven times so the face sheet thickness h_f ranges from 0.772 to 5.404 mm (from 0.03" to 0.21"). All face sheets were modeled with one solid brick element through the thickness, where a composite layered section was specified in the element with a different material orientation for each ply through the thickness [17]. The material properties of the individual ply were based on the NCAMP material qualification [18]. Hexcel HRH-10®[3] honeycomb core consisting of NOMEX®[4] paper with 29, 48 and 80 kg/m^3 (1.8 , 3.0 and 5.0 lb/ft^3) density and 3.2 mm (0.125") cell size was chosen as core material [19]. In this study, the core thickness h_c ranges from 12.7 to 76.2 mm (from 0.5" to 3"). The material properties are shown in Table 1 and the parameter matrix for all investigated analysis configurations in Table 2.

The pressure-deformation coupling was simulated with the use of a surface based fluid cavity. This ABAQUS®/Standard feature enabled the definition of fluid-filled cavities enclosed by structural elements. The ideal gas law, given in Eq. 1, was solved within each increment until equilibrium was found between pressure, volume, and temperature by coupling the internally defined fluid elements with the surrounding structural elements [17]. As mentioned in the introduction, the volume fraction of the honeycomb cell walls was very small. For this reason, the volume of the fluid cavities was assumed to be equal to that of the actual sandwich core. Two separate cavities are defined for the disbonded and for the intact core section, as shown in Figure 2. Directly at the crack front, the cells become completely connected to the disbonded cavity, as soon as the crack reaches their edge. Consequently, the pressure in the cells directly below the crack tip is the same as the pressure in the disbonded part. For this reason, the border between the intact and disbonded cavity is shifted by one cell size to the front of the crack tip, as shown in the enlarged insert of Figure 2 (dashed blue line). For the analysis, the initial and ambient conditions had to be defined. An aircraft ascent scenario was considered from 0 to 12192 m (0 to 40000 ft). From the International Standard Atmosphere, the initial values for the intact and disbonded sections before take off and the ambient values at 12192 m [20] were obtained:

[2] CYCOM® is a product of Cytec Industries Inc., Woodland Park, NJ, USA

[3] Hexcel HRH-10® is a product of Hexcel Corporation, Stamford, CT, USA

[4] NOMEX® is a product of E. I. du Pont de Nemours and Company, Wilmington, DE, USA

$$p_{\text{int},0} = p_{\text{deb},0} = p_{\text{a},0} = p(0\,\text{m}) = 0.1013\,\text{MPa} \tag{2}$$

$$T_{\text{int},0} = T_{\text{deb},0} = T_{\text{a},0} = T(0\,\text{m}) = 288.15\,\text{K} \tag{3}$$

$$p_{\text{a},1} = p(12193\,\text{m}) = 0.0188\,\text{MPa} \tag{4}$$

$$T_{\text{int},1} = T_{\text{deb},1} = T_{\text{a},1} = T(12193\,\text{m}) = 216.65\,\text{K} \tag{5}$$

The temperature in the core was assumed and defined equal to the ambient temperature, whereas pressure and volume inside the cavities were calculated during the analysis.

The total energy release rate at the crack tip along the disbond front was calculated using the Virtual Crack Closure Technique (VCCT) using a user-written post-processing routine [12]. The analysis requires access to the element forces at nodes along the crack front and the nodal displacements one row behind the front. The nodal point coordinates are also required to calculate the area virtually closed. This input data for the routine are extracted directly from an ABAQUS®/Standard binary result file (.fil). Details can be found in an earlier report [21].

4. Validation of the Modeling Technique

Before the parameteric study was performed, the modeling technique discussed above was validated by simulating two different internally pressurized sandwich panels taken from previous investigations [5, 6, 10, 11].

4.1 Investigation Program of the X-33 Liquid Hydrogen Tank Failure

The failure of the sandwich liquid hydrogen tank during the full-scale test of the X-33 technology flight demonstration vehicle due to face sheet disbonding, which was caused by pressure difference, environmental effects, and initial disbonds, is described in detail in the final report of the investigation team [5]. In a series of tests, the investigation team pressurized the core of several sandwich panels containing initial disbonds using a compressor and measured the failure pressure when the face sheet disbonded from the core. They then simulated this test using finite element analyses and calculated the energy release rate along the initial disbond front by applying VCCT. The computed mode I component was dominant (G_{II} was reported to be less than 10% G_I) and the results were compared with experimentally determined fracture toughness values obtained from Single Cantilever Beam specimens [6].

Since the cell walls of the KOREX®[5] honeycomb core were perforated, the pressure could be assumed equal everywhere in the panel. Therefore, no pressure-deformation coupling effect occurred and the pressure was defined by the compressor. Consequently, the pressure could be applied as a constant load at the nodes of the inner and outer face sheets of the sandwich panel.

In order to validate the pressure application in the sandwich core using ABAQUS® Fluid Cavity and the calculation of the energy release rate by applying VCCT, the X-33 sandwich panel was modeled as described in the previous section. The only differences were the materials used and the shape of the disbond (rectangular instead of a circular disbond between the inner face sheet and the core). The materials and their respective properties are described by Glaessgen et.al. [6] and listed in Table 3. The FE model is shown in Figure 3. The panel is a_p = 305 mm (12.0") long and b_p = 305 mm (12.0") wide. The inner (disbonded) face sheet is h_{fi} = 1.78 mm (0.07"), the core h_c = 38.1 mm (1.5") and the outer face sheet h_{fo} = 0.86 mm (0.034") thick. Three disbonds with a_{disb} = 12.7, 25.4 and 38.1 mm (0.5, 1.0 and 1.5") length and b_{disb} = 76.2 mm (3.0") width were simulated. Since the pressure was equal everywhere in the sandwich core, only one cavity was needed for the pressure application during the analysis. The pressure loads defined for the cavities were p = 552 kPa (80 psi) and 827 kPa (120 psi) respectively [6].

Figure 4 shows the total energy release rate, G_T (solid lines), along the disbond front (at the y-axis) for two pressure levels. As expected, G_T increases with the applied pressure and the disbond length. These data were compared to those published by Glaessgen et.al. [6]. In order to provide a more meaningful comparison with computed G_T, the data from Glaessgen were scaled. Based on the fact that G_I was reported to be dominant and G_{II} was approximately 10% of G_I, the data were scaled by a factor of 1.1 (dashed lines in Figure 4). The current results correlate well with the scaled values of G_T. Overall, the pressure application using the fluid cavity in combination with the VCCT calculation, gave acceptable results.

4.2 Investigation Program of the Airbus Rudder Failure during Air Transat Flight 961

During Air Transat Flight 961, the sandwich rudder of an Airbus A310-308 failed due to large scale face sheet/core disbonding caused by the combination of initial disbonds and the increasing core pressure during ascent. The incident, and its investigation, are described in detail in the final report of the Canadian aviation authority [10]. During the investigation program, a sandwich panel with a circular disbond between face sheet and core was tested in a

[5] KOREX® is a product of E. I. du Pont de Nemours and Company, Wilmington, DE, USA

vacuum chamber to simulate the pressure difference in and outside of the sandwich during ascent. The disbond radius of the square panel was r_{disb} = 175.0 mm (6.89”). The sandwich was symmetric with a h_c = 40 mm (1.575”) core height and a h_f = 0.48 mm (0.019”) face sheet thickness. During the test, the pressure in and outside of the sandwich was measured. The test details were presented by Hilgers [11]. The face sheet layup and the material properties were provided by Airbus, however, were not released for publication.

Since a non-vented NOMEX® honeycomb core is used in this sandwich structure, the modeling assumptions and conditions were exactly the same as described in section 2 and 3. The face sheets were quite thin and the pressure-deformation coupling needed to be taken into account to simulate the deformation and the bulging of the panel. The investigation team simulated the test and solved the pressure-deformation coupling iteratively with an ANSYS®[6] subroutine developed specifically for this purpose. In the disbonded sandwich section, they measured a pressure of 0.0582 MPa during the test and calculated 0.0577 MPa with the finite element analysis [11].

To validate the current modeling technique and the solution of the pressure-deformation coupling problem by using the ABAQUS® fluid cavity feature, the test was reanalyzed. The modeling assumptions were described previously and the FE model is identical to the one presented in Figure 2. Using the current approach, the pressure in the disbonded section was calculated as 0.0571 MPa. The difference is only about 1 % compared to the presented simulation results [11]. The results confirm the suitability of the current modeling technique for pressurized sandwich structures.

5. Analysis results for simulated ground-air pressurization

Two analysis series were performed to investigate the influence of the disbond radius, the face sheet thickness, the core height and of the core density on the bulging of the disbonded sandwich and the crack tip loading along the disbond front. In the first series, the core thickness was kept constant at 25.4 mm (1.0”) and in the second, the core density at 48 kg/m^3 (3.0 lb/ft^3). The sets of analyses that were performed are listed in Table .

5.1 Effect of core density, disbond radius and face sheet thickness on sandwich deformation and disbond loading conditions

In the first analysis series, the disbond radius ranged from 50.8 to 152.4 mm (from 2.0 to 6.0”) and the face sheet thickness from 0.772 to 5.404 mm (from 0.03 to 0.21”). With 29, 48 and

[6] ANSYS® is a product of ANSYS, Inc., Canonsburg, PA, USA

80 kg/m^3 (1.8, 3.0 and 5.0 lb/ft^3), three different densities of the Hexcel HRH-10® 1/8 honeycomb core were investigated. The core was always 25.4 mm (1.0") thick.

Figures 5 and 6 show polar diagrams with the energy release rate G_T along the disbond front in the sandwich panel with the smallest disbond and the thickest face sheets and in the sandwich panel with the largest disbond and the thinnest face sheets, respectively. The combination of the thickest face sheets and the smallest disbond results is the safest case (lowest valus of G_T). Due to the high face sheet bending stiffness and the small bending area, the bulging of the disbonded sandwich is negligible. Consequently, the crack opening is insignificant and the crack tip loading very low. The most critical case is the configuration with the largest disbond and the thinnest face sheets. Here, significant bulging occurs and the crack opening results in a higher crack tip loading. This becomes apparent by comparing the results shown in Figures 5 and 6. With the thinnest face sheet and the largest disbond, the energy release rate G_T is 100 times higher than with the smallest disbond and the thickest face sheet. The core density seems to have an effect in the safest case. G_T of the low density core sandwich is a factor of two higher than in the high density core sandwich. However, the difference disappears almost completely in the most critical configuration.

For better understanding, the results of the first analysis loop are presented as surface plots. The bulging of the disbonded sandwich part is defined by the relative volume increase V_1/V_0, shown in Figure 7. It becomes apparent, that the core density (within the range investigated here) doesn't affect the global deformation behavior. The three results fall basically on top of each other. Consequently, the pressure decrease caused by the bulging (Figure 8) is also independent of the core density. Figure 9 shows the maximum G_T along the crack front, which occurs in almost all cases at or close to the 45°-axis between the x- and the y-axis (as shown in Figures 5 and 6). As already discussed, the effect of the core density on G_T is significant only for the small disbond/thick face sheet configuration when G_T is very small anyway. For almost all configurations, the crack tip loading G_T is nearly independent of the core density, as shown in Figure 9.

The dependency of the crack tip loading on the bulging of the disbonded sandwich part becomes apparent when comparing the results in Figure 7 and 9. The total energy release rate, G_T, becomes significant only in the case of severe bulging and relative volume increase. On the other hand, due to the ideal gas law, the pressure load (shown in Figure 8) becomes minimal when the relative volume increase and G_T are at a maximum. Hence, for the current configurations considered, the computed crack tip loading is a maximum when the internal pressure loading is minimal. The computed crack tip loading would have been even higher had the pressure-deformation coupling and the pressure decrease not been considered during the analysis.

5.2 Effect of core thickness on sandwich deformation and disbond loading conditions

In the second analysis series, the disbond radius ranged again from 50.8 to 152.4 mm (from 2.0 to 6.0”) and the face sheet thickness from 0.772 to 5.404 mm (from 0.03 to 0.21”). The core thicknesses investigated were 12.7, 25.4, 50.8 and 76.2 mm (0.5, 1.0, 2.0 and 3.0”) while the core density was held constant at 48 kg/m^3 (3.0 lb/ft^3).

For all core heights considered, the results have qualitatively the same effect as described in the previous section. However, the magnitude of the pressure-deformation coupling effects is strongly affected by the core thickness, as shown in Figures 10 through 12. Since the bulging of the disbonded sandwich part is mainly driven by the bending capacity of the face sheets and less by the sandwich core, the absolute volume increase, $V_1 - V_0$, is nearly independent of the core thickness. Consequently, as shown in Figure 10, the relative volume increase V_1/V_0 is much higher for thin cores with small initial volume V_0 than for thick core configurations with large V_0. For the most critical combination with 152.4 mm disbond radius and 0.772 mm face sheet thickness, the relative volume increase is only 1.09 at 76.2 mm and 1.52 in case of 12.7 mm core thickness. This results in a more intensive pressure decrease in the thin core configuration, visible in Figure 11. In the deformed disbonded sandwich part, the pressure is 0.051 MPa in the 76.2 mm configuration and only 0.031 MPa with 12.7 mm core thickness. The significant lower pressure load results also in a lower crack front loading, visible in Figure 12. The maximum G_T is 651 J/m² in the 76.2 mm configuration and 322 J/m² with 12.7 mm core thickness.

Overall, the pressure-deformation related effects are more relevant in sandwich configurations with thin cores. Furthermore, the internal pressurization caused by decreasing ambient pressure is less critical in thin core configurations than in thick core configurations.

5.3 Effect of large disbonds on disbond loading conditions

As discussed in the previous section, the total energy release rate, G_T, increases for all configurations considered when the disbond radius increased and the face sheet thickness decreased. Therefore, if G_T exceeds the fracture toughness, the disbond propagation would always occur under unstable conditions. However, as shown in Figure 12, the total energy release rate, G_T, decreases for larger disbonds, thinner face sheets, and thinner cores. This is caused by the significant pressure load decrease due to large-scale bulging described in the last section.

To investigate G_T and its slope at very large disbonds, analyses were performed with various disbond radii up to 762 mm (30.0”), five times larger than in the previous sections. The core and face sheet were 25.4 and 0.772 mm (1.0 and 0.03”) thick, respectively. Figure 13 shows the

pressure in the disbonded sandwich section as a function of the disbond radius. The pressure load decreases asymptotically down to the ambient pressure. In theory, the ambient pressure and the pressure in the disbonded sandwich section become equal at an infinite disbond radius. The significant pressure decrease causes a distinct abatement of the slope of G_T, visible in Figure 14. At about 420 mm disbond radius, the slope becomes zero and with further disbond increase even negative. This means, that the crack tip is increasingly unloaded for increasing disbond radius (above 420 mm). Assuming face sheet/core interface fracture toughness is independent of the disbond length, this result indicates that disbond propagation would become stable at disbond radii exceeding 420mm. On the other hand, a minimum fracture toughness can be derived from this analysis to prevent face sheet/core disbond propagation. Figure 14 shows G_T always below 880 J/m^2. If the face sheet/core interface fracture toughness is higher than this design limit, no disbond propagation would occur regardless of the disbond size.

6. Conclusions

In this study, the criticality of face sheet/core disbonds of honeycomb sandwich aircraft structures loaded by internal pressurization due to decreasing ambient pressure during ascent was investigated. Finite element analyses were performed and the disbond front loading in terms of the energy release rate was calculated using the Virtual Crack Closure Technique. The recursive pressure-deformation coupling within the disbonded sandwich core following the ideal gas law was taken into account during the analyses by applying ABAQUS® fluid cavities. Both, the pressure-deformation coupling and the calculation of the crack tip loading, were validated by comparing computed results to values from two previously published case studies.

For the numerical study, a square sandwich panel was considered having a circular disbond between one face sheet and the core. As expected, large disbonds are more critical than smaller ones. The face sheet thickness was identified as another important parameter. Thin face sheets having a low bending stiffness cause more bulging of the disbonded sandwich section. Consequently, the face sheet/core opening and so the crack tip loading are higher compared to results obtained from analyses of thick face sheet configurations.

The analyses have shown that the pressure-deformation coupling has an effect, especially for the most critical configurations with thin face sheets and large disbonds. In this case, the large-scale bulging causes a significant volume increase and, following the ideal gas law, a decrease of the internal pressure load. The pressure decrease finally results in a lower loading at the disbond front. Without considering the lower pressure, the crack tip loading for the most critical configurations would be even higher. Since the pressure drop is driven by the relative

volume increase and not by the absolute volume increase, the pressure-deformation coupling is more important for sandwich configurations with thin cores. Thus, the core thickness was identified as the third important parameter. The pressure load and consequently the crack front loading are higher in sandwich configurations with thick cores.

The observed large-scale bulging for large disbonds causes a significant decrease in pressure. Therefore, once a critical disbond radius is exceeded, the crack front loading does not increase but decreases. The disbond propagation will change from unstable to stable and finally stop. Consequently, the crack front loading has a defined maximum depending on the sandwich configuration and the initial and ambient pressure. Provided that the face sheet/core interface fracture toughness remains above this design limit, no disbond propagation will to occur, regardless of the initial disbond size.

Acknowledgements

This work was supported by the fellowship program PROF.x^2 of Fraunhofer-Gesellschaft zur Förderung der angewandten Forschung e.V. The work was performed while Dr. Rinker was a visiting scientist at the National Institute of Aerospace (NIA).

The analyses were performed at the Durability, Damage Tolerance and Reliability Branch at NASA Langley Research Center, Hampton, Virginia, USA.

References

1. Vinson JR. Sandwich Structures: “Past, Present, and Future. In: Sandwich Structures 7: Advancing with Sandwich Structures and Materials,” Proceedings of the 7th International Conference on Sandwich Structures, Aalborg, Denmark, 29-31 August 2005, pp. 3-12.

2. Herrmann AS, Zahlen PC and Zuardy I: “Sandwich Structures Technology in Commercial Aviation. In: Sandwich Structures 7: Advancing with Sandwich Structures and Materials,” Proceedings of the 7th International Conference on Sandwich Structures, Aalborg, Denmark, 29-31 August 2005, pp. 13-26.

3. Low GM. Apollo 6 Anomaly Report No. 6: “Abnormal Structural Performance During Launch Phase,” NASA-TM-X-70374, National Aeronautics and Space Administration, Houston, TX, USA, April 1969.

4. Epstein G and Ruth S. “Honeycomb Sandwich Structures: Vented Versus Unvented Designs for Space Systems,” Aerospace Report No. TR-93(3904)-1, The Aerospace Corporation, El Segundo, CA, USA, October 1993.

5. Goetz et al. “Final Report of the X-33 Liquid Hydrogen Tank Test Investigation Team,” National Aeronautics and Space Administration, Huntsville, AL, USA, May 2000.

6. Glaessgen EH, Reeder JR, Sleight DW, Wang JT, Raju IS and Harris CE: “Debonding. Failure of Sandwich-Composite Cryogenic Fuel Tank with Internal Core Pressure,” Journal of Spacecraft and Rockets 2005, vol. 42, no. 4, pp. 613-627.

7. Air Accident Investigation Branch. AAIB Bulletin 8/92 Ref: EW/A92/5/1, Air Accident Investigation, UK, 1992.

8. Air Accident Investigation Branch. AAIB Bulletin 2/95 Ref: EW/C94/8/3, Air Accident Investigation, UK, 1995.

9. Air Accident Investigation Branch. AAIB Bulletin 10/96 Ref: EW/C96/6/6, Air Accident Investigation, UK, 1996.

10. Transportation Safety Board of Canada. Aviation Investigation Report A05F0047, Minister of Public Works and Government Services Canada, 2007.

11. Hilgers R: “Substantiation of Damage Growth within Sandwich Structures,” FAA Workshop for Composite Damage Tolerance & Maintenance, Tokyo, Japan, 1-5 June 2009.

12. Rybicki EF and Kanninen MF: “A Finite Element Calculation of Stress Intensity Factors by a Modified Crack Closure Integral,” Engineering Fracture Mechanics 1977, vol. 9, no. 4, pp. 931-938.

13. Krueger R: “Virtual Crack Closure Technique: History, Approach, and Applications,” Applied Mechanics Reviews 2004, vol. 57, no. 2, pp. 109-143.

14. Sun CT and Jih CJ: “On Strain Energy Release Rates for Interfacial Cracks in Bi-Material Media,” Engineering Fracture Mechanics 1987, vol. 28, no. 1, pp. 13-20.

15. Carlsson L and S. Prasad: “Interfacial Fracture of Sandwich Beams,” Engineering Fracture Mechanics 1993, vol. 44, no. 4, pp. 581-590.

16. Glass DE, Raman VV, Venkat VS and Sankaran SN: “Graphite/Epoxy Honeycomb Core Sandwich Permeability Under Mechanical Loads,” Composite Structures 1999, vol. 44, no. 4, pp. 253-261.

17. ABAQUS® 6.12 Documentation. Providence, RI, USA: Dassault Systemes Simulia Corporation; 2012.

18. National Center for Advanced Materials Performance (NCAMP), www.niar.wichita.edu/coe/ncamp.

19. HexWeb™ Honeycomb Attributes and Properties. Material Data Sheet, Hexcel Composites, 1999.

20. ISO 2533:1975 Standard Atmosphere. International Organization for Standardization.

21. Krueger R and Goetze D: "Influence of Finite Element Software on Energy Release Rates Computed Using the Virtual Crack Closure Technique," NIA Report No. 2006-06, NASA/CR-2006-214523, 2006.

Tables

	E_{11} [MPa]	E_{22} [MPa]	E_{33} [MPa]	G_{12} [MPa]	G_{13} [MPa]	G_{23} [MPa]	ν_{12} -	ν_{13} -	ν_{23} -
CYCOM® 5320PW	64663.	63250.	10748.	5064.	3624.	3824.	0.053	0.516	0.512
HRH-10® 1.8-1/8	0.1	0.1	55.1	0.1	10.3	26.2	0.3	1e-06	1e-06
HRH-10® 3.0-1/8	0.1	0.1	137.8	0.1	24.1	44.8	0.3	1e-06	1e-06
HRH-10® 5.0-1/8	0.1	0.1	254.9	0.1	37.2	70.3	0.3	1e-06	1e-06

Table 1: Material Properties for the Parametric Study.

Core density	Core thickness	Face sheet thickness	Disbond radius
29.0 kg/m^3 (1.8 lb/ft^3)	25.4 mm (0.5”)	0.772, 1.544, 2.316, 3.088, 3.860, 4.632, 5.404 mm (0.03, 0.06, 0.09, 0.12, 0.15, 0.18, 0.21”)	50.8, 101.6, 152.4 mm (2.0, 4.0, 6.0”)
48.0 kg/m^3 (3.0 lb/ft^3)	12.7 mm (0.5”)	0.772, 1.544, 2.316, 3.088, 3.860, 4.632, 5.404 mm (0.03, 0.06, 0.09, 0.12, 0.15, 0.18, 0.21”)	50.8, 101.6, 152.4 mm (2.0, 4.0, 6.0”)
48.0 kg/m^3 (3.0 lb/ft^3)	25.4 mm (1.0”)	0.772, 1.544, 2.316, 3.088, 3.860, 4.632, 5.404 mm (0.03, 0.06, 0.09, 0.12, 0.15, 0.18, 0.21”)	50.8, 101.6, 152.4 mm (2.0, 4.0, 6.0”)
48.0 kg/m^3 (3.0 lb/ft^3)	25.4 mm (1.0”)	0.772 mm (0.03”)	203.2, 254.0, 304.8, 355.6, 406.4, 457.2, 508.0, 558.8, 609.6, 660.4, 711.2, 762.0 mm (8.0, 10.0, 12.0, 14.0, 16.0, 18.0, 20.0, 22.0, 24.0, 26.0, 28.0, 30.0”)
48.0 kg/m^3 (3.0 lb/ft^3)	50.8 mm (2.0”)	0.772, 1.544, 2.316, 3.088, 3.860, 4.632, 5.404 mm (0.03, 0.06, 0.09, 0.12, 0.15, 0.18, 0.21”)	50.8, 101.6, 152.4 mm (2.0, 4.0, 6.0”)
48.0 kg/m^3 (3.0 lb/ft^3)	76.4 mm (3.0”)	0.772, 1.544, 2.316, 3.088, 3.860, 4.632, 5.404 mm (0.03, 0.06, 0.09, 0.12, 0.15, 0.18, 0.21”)	50.8, 101.6, 152.4 mm (2.0, 4.0, 6.0”)
80.0 kg/m^3 (5.0 lb/ft^3)	25.4 mm (1.0”)	0.772, 1.544, 2.316, 3.088, 3.860, 4.632, 5.404 mm (0.03, 0.06, 0.09, 0.12, 0.15, 0.18, 0.21”)	50.8, 101.6, 152.4 mm (2.0, 4.0, 6.0”)

Table 2: Parameter matrix for all investigated analysis configurations.

	E_{11} [MPa]	E_{22} [MPa]	E_{33} [MPa]	G_{12} [MPa]	G_{13} [MPa]	G_{23} [MPa]	ν_{12} -	ν_{13} -	ν_{23} -
Inner face sheet	19300.	77900.	6900.	13310.	5500.	5500.	0.125	0.25	0.25
KOREX® - core	4.0	4.0	140.0	4.0	15.9	74.5	0.25	0.02	0.02
Outer face sheet	47640.	43300.	6900.	10890.	5500.	5500.	0.202	0.25	0.25

Table 3: Material Properties of the X-33 sandwich panel.

Figures

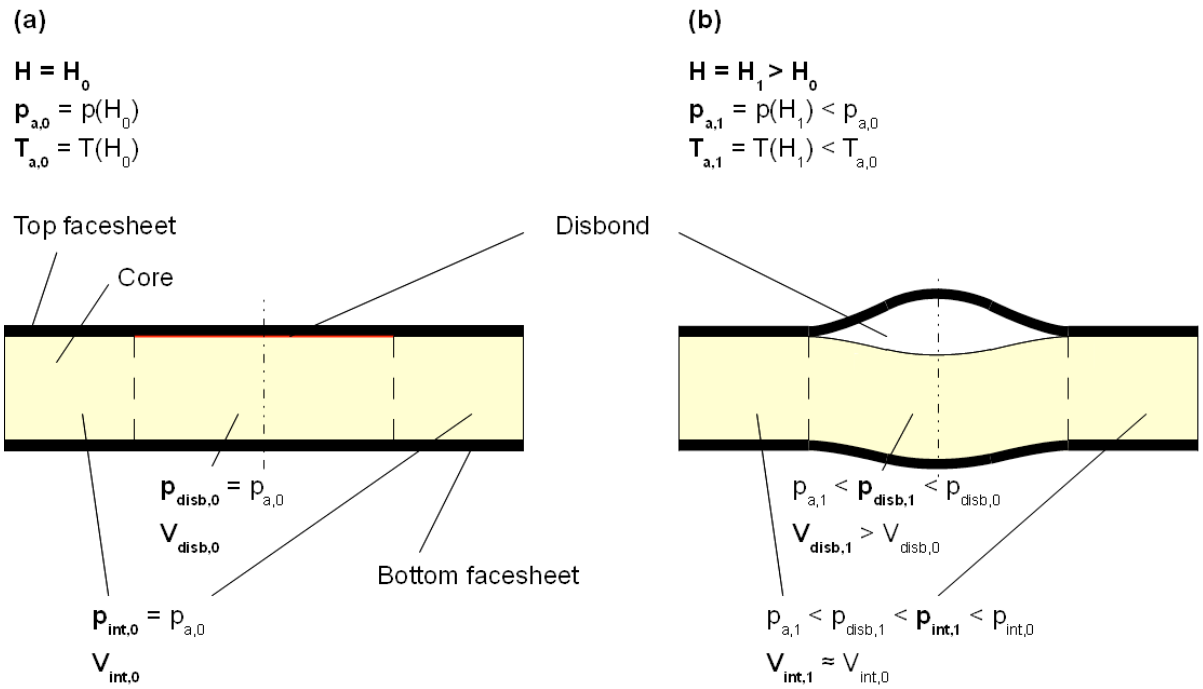

Figure 1: Deformation and pressure behavior of a honeycomb sandwich sandwich panel with circular disbond on ground (a) and at flight altitude (b).

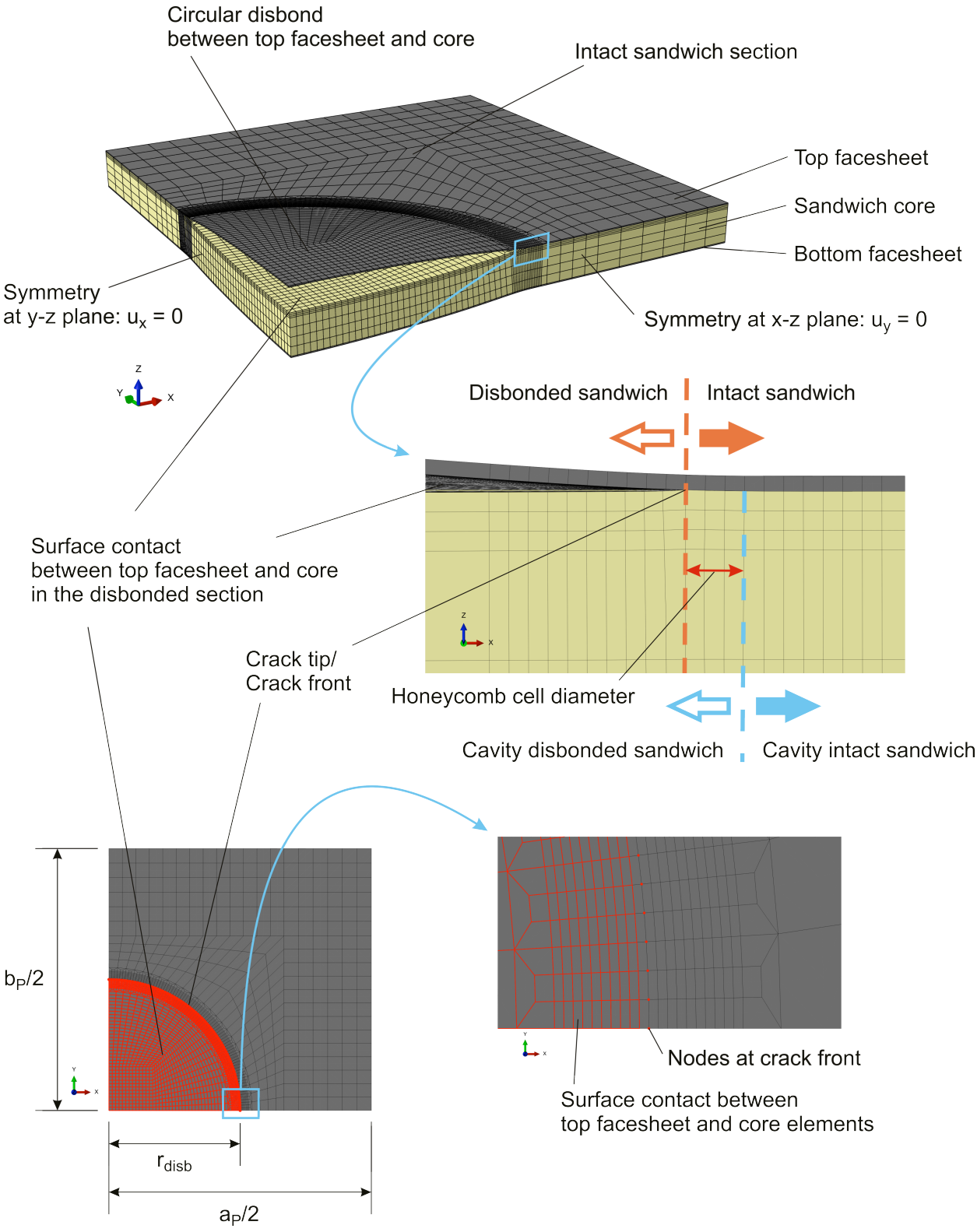

Figure 2: Finite Element Model for the Parameter Study.

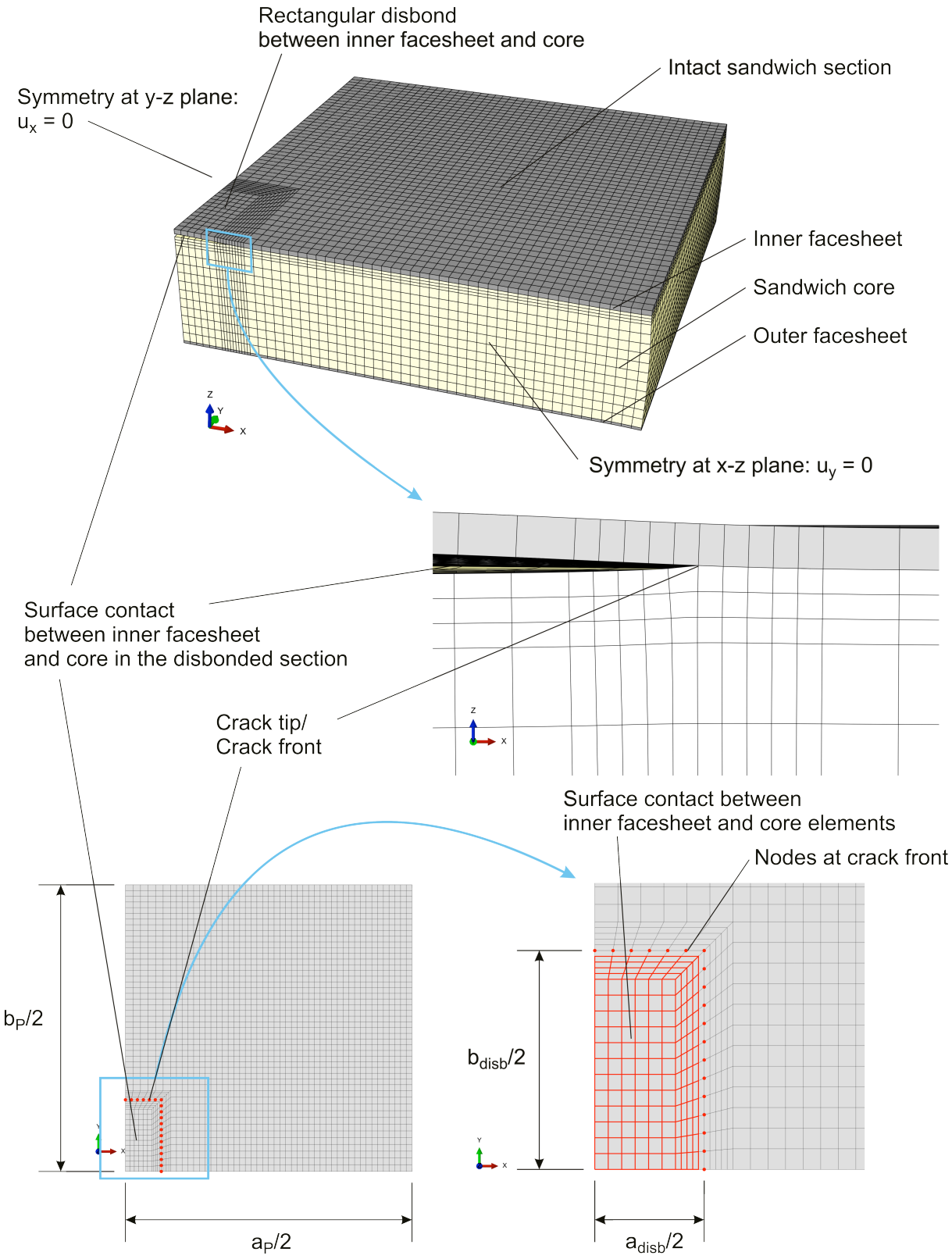

Figure 3: Finite Element Model of the Pressurized X-33 Sandwich Panel.

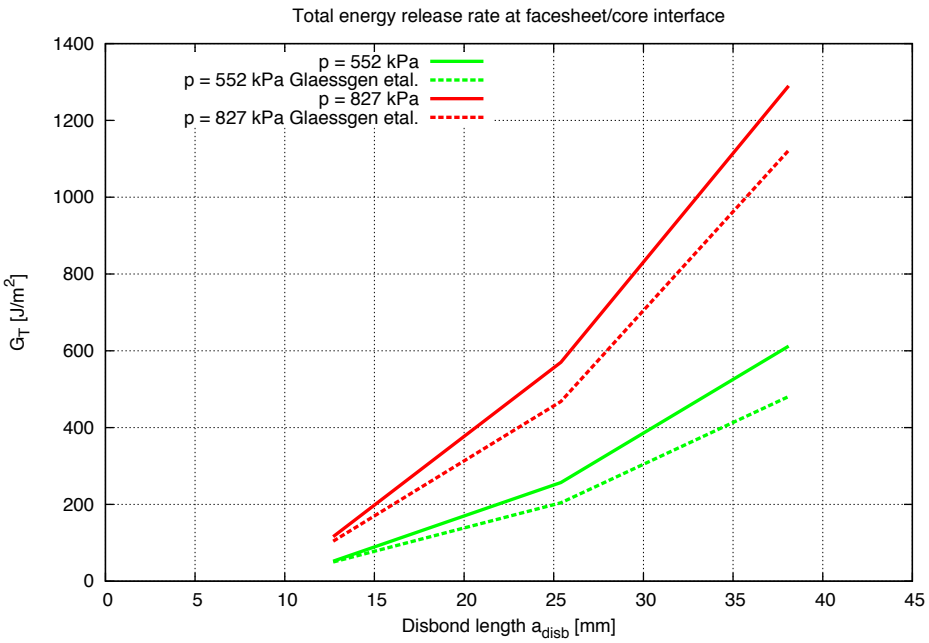

Figure 4: Mode I energy release rate at the disbond front in the pressurized X-33 sandwich panel.

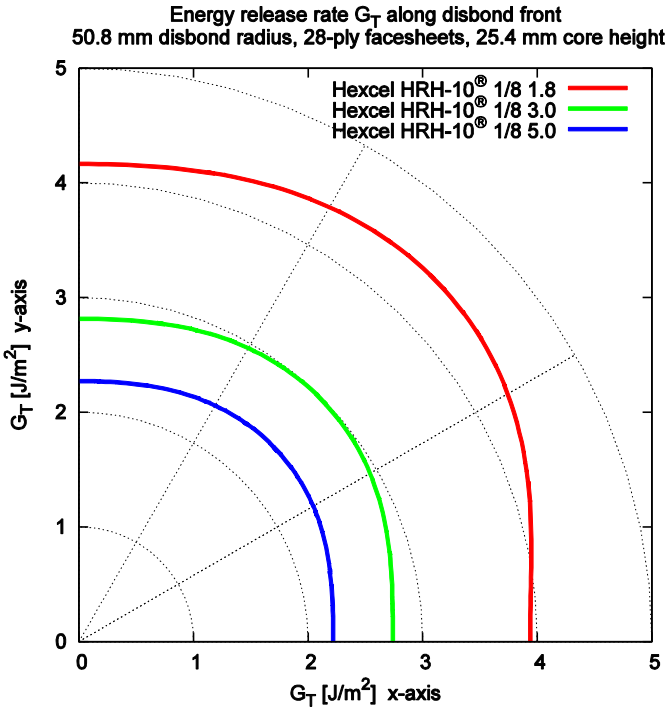

Figure 5: Energy release rate G_T along disbond front in the sandwich panel with 50.8 mm disbond radius, 28-ply face sheets, 25.4 mm core thickness and different core densities.

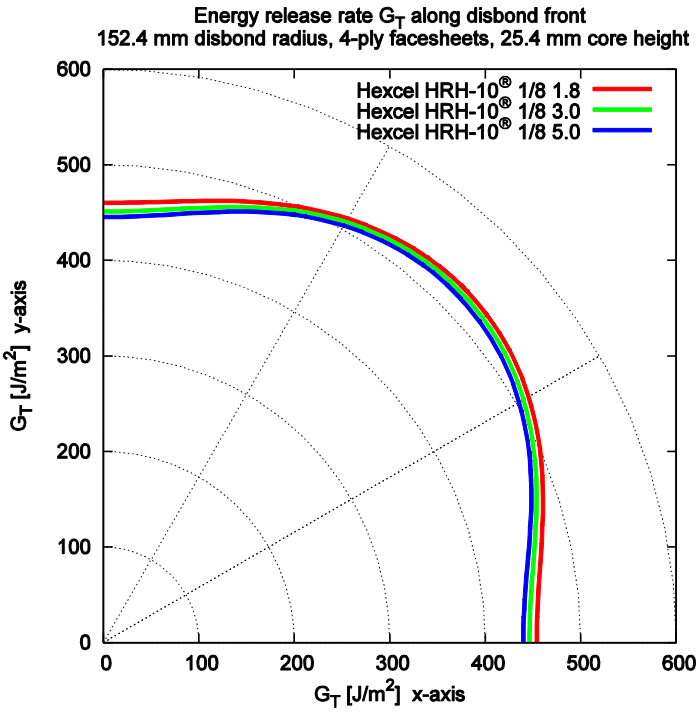

Figure 6: Energy release rate G_T along disbond front in the sandwich panel with 152.4 mm disbond radius, 4-ply face sheets, 25.4 mm core thickness and different core densities.

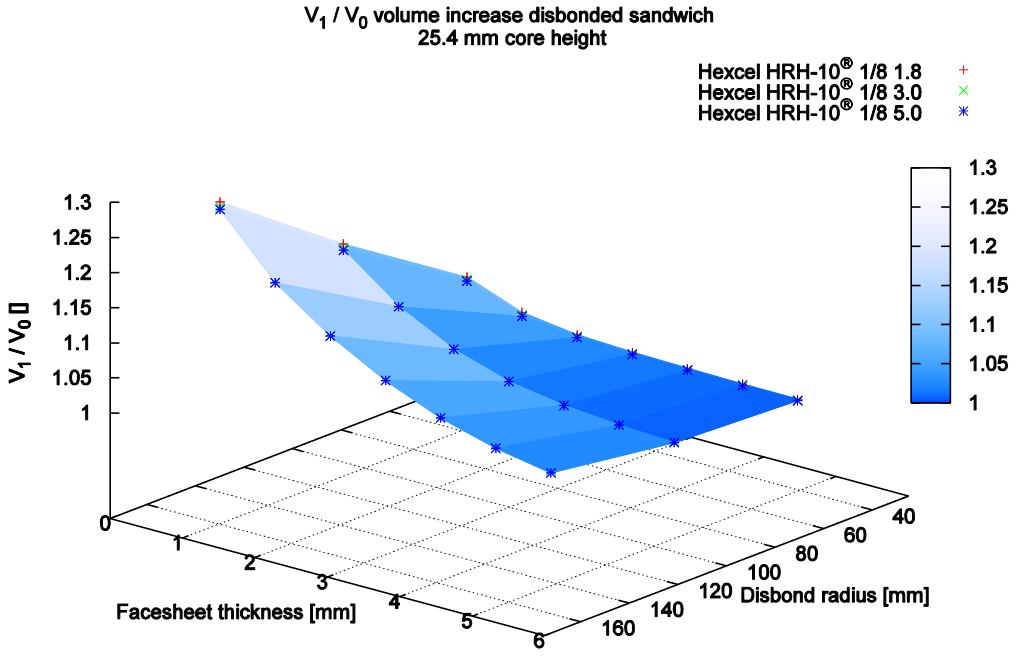

Figure 7: Relative volume increase of the disbonded sandwich core due to internal pressurization as a function of the disbond radius r_{disb} and the face sheet thickness h_f for different core densities.

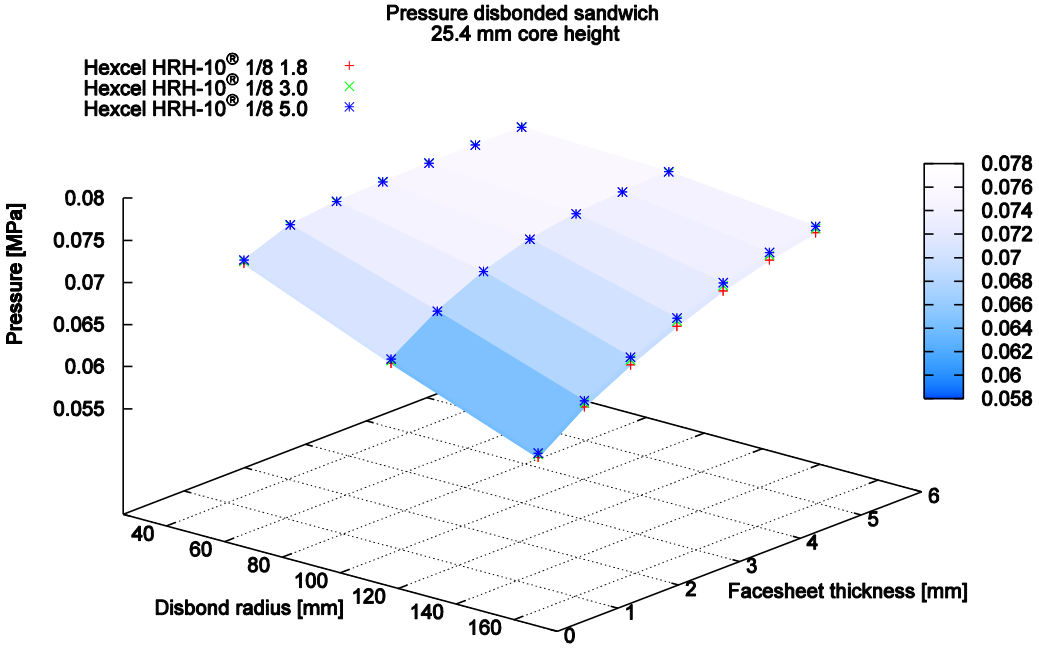

Figure 8: Pressure decrease in the disbonded sandwich core due to bulging and volume increase as a function of the disbond radius r_{disb} and the face sheet thickness h_f for different core densities.

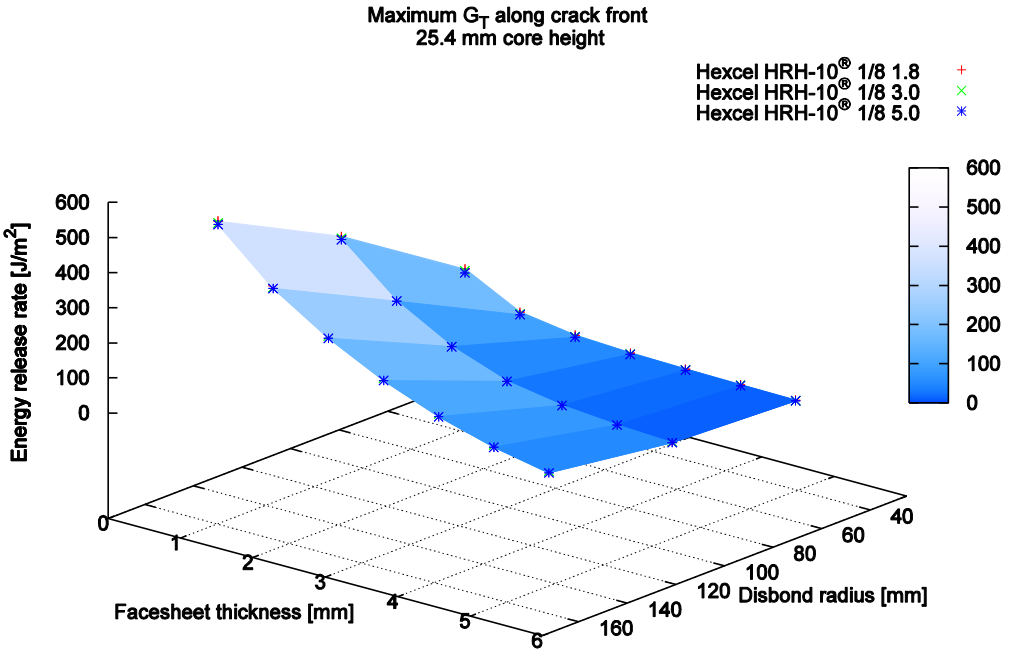

Figure 9: Maximum crack tip loading G_T along the disbond front as a function of the disbond radius r_{disb} and the face sheet thickness h_f for different core densities.

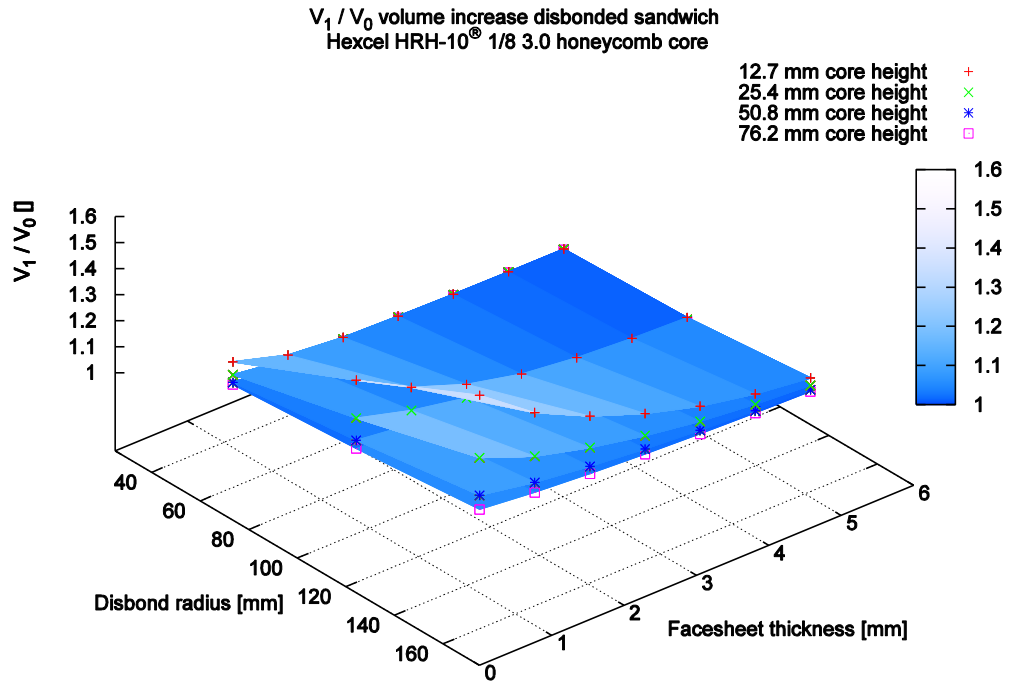

Figure 10: Relative volume increase of the disbonded sandwich core due to internal pressurization as a function of the disbond radius r_{disb} and the face sheet thickness h_f for different core thicknesses.

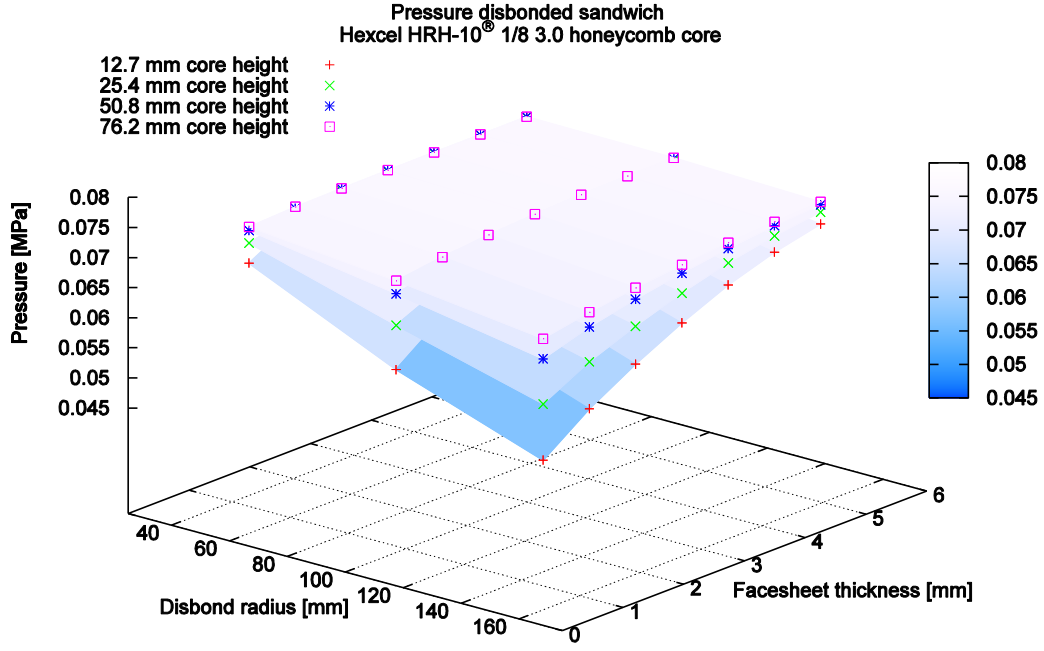

Figure 11: Pressure decrease in the disbonded sandwich core due to bulging and volume increase as a function of the disbond radius r_{disb} and the face sheet thickness h_f for different core thicknesses.

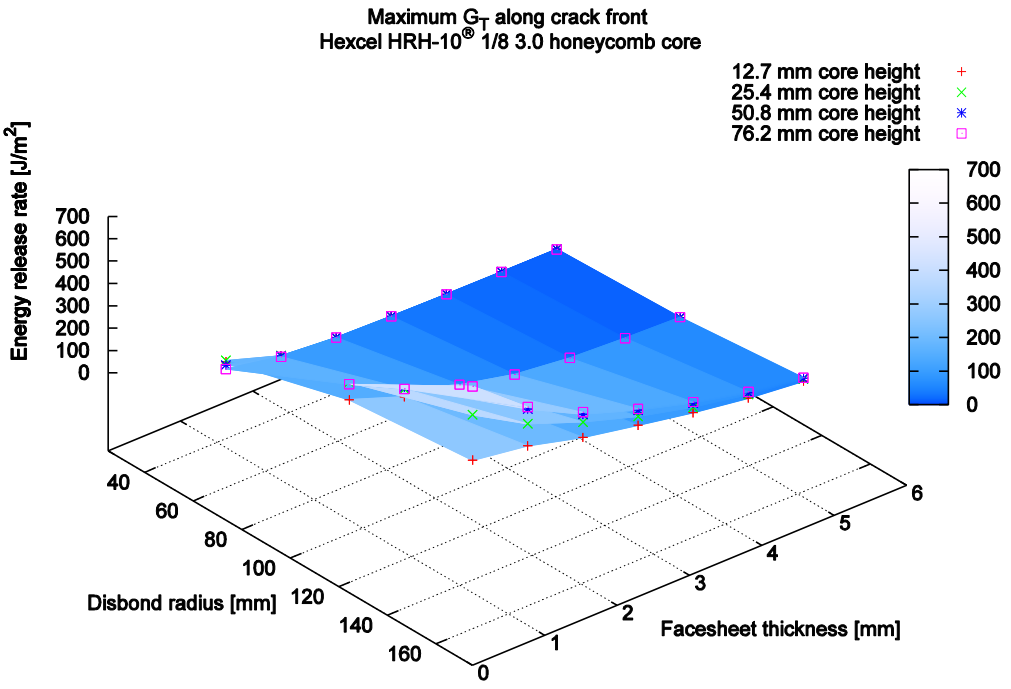

Figure 12: Maximum crack tip loading G_T along the disbond front as a function of the disbond radius r_{disb} and the face sheet thickness h_f for different core thicknesses.

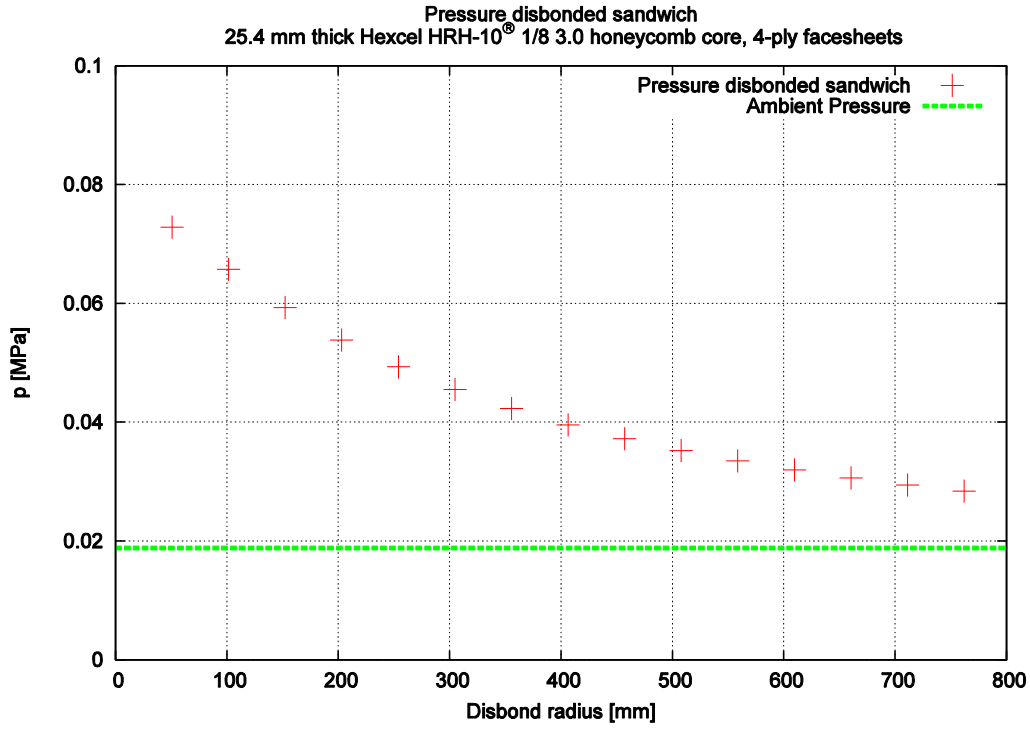

Figure 13: Pressure decrease in the disbonded sandwich section at large disbonds.

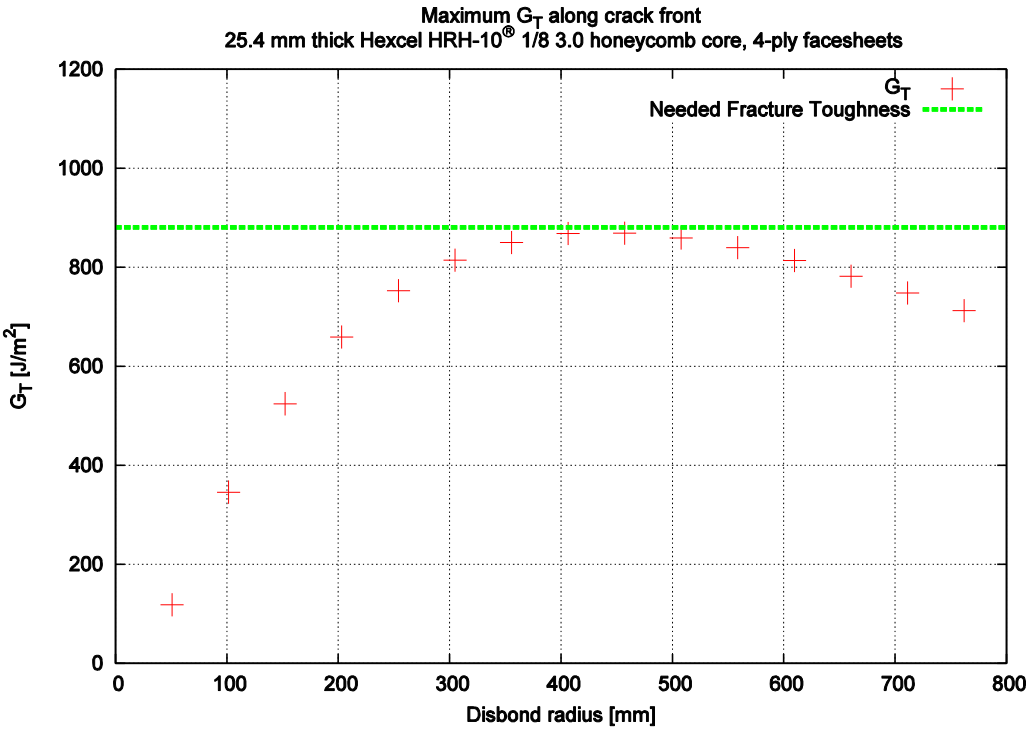

Figure 14: Maximum crack tip loading G_T along the disbond front at large disbonds.

REPORT DOCUMENTATION PAGE

Form Approved
OMB No. 0704-0188

1. REPORT DATE *(DD-MM-YYYY)*	2. REPORT TYPE	3. DATES COVERED *(From - To)*
01- 03 - 2013	Contractor Report	

4. TITLE AND SUBTITLE

Analysis of an Aircraft Honeycomb Sandwich Panel with Circular Face Sheet/Core Disbond Subjected to Ground-Air Pressurization

5a. CONTRACT NUMBER

5b. GRANT NUMBER

NNL09AA00A

5c. PROGRAM ELEMENT NUMBER

6. AUTHOR(S)

Rinker, Martin; Krueger, Ronald; Ratcliffe, James G.

5d. PROJECT NUMBER

5e. TASK NUMBER

5f. WORK UNIT NUMBER

794072.02.07.03.03

7. PERFORMING ORGANIZATION NAME(S) AND ADDRESS(ES)

NASA Langley Research Center
Hampton, Virginia 23681

8. PERFORMING ORGANIZATION REPORT NUMBER

NIA Report No. 2013-0116

9. SPONSORING/MONITORING AGENCY NAME(S) AND ADDRESS(ES)

National Aeronautics and Space Administration
Washington, DC 20546-0001

10. SPONSOR/MONITOR'S ACRONYM(S)

NASA

11. SPONSOR/MONITOR'S REPORT NUMBER(S)

NASA/CR-2013-217974

12. DISTRIBUTION/AVAILABILITY STATEMENT

Unclassified - Unlimited
Subject Category 24
Availability: NASA CASI (443) 757-5802

13. SUPPLEMENTARY NOTES

Langley Technical Monitor: Jonathan B. Ransom

14. ABSTRACT

The ground-air pressurization of lightweight honeycomb sandwich structures caused by alternating pressure differences between the enclosed air within the honeycomb core and the ambient environment is a well-known and controllable loading condition of aerospace structures. However, initial face sheet/core disbonds intensify the face sheet peeling effect of the internal pressure load significantly and can decrease the reliability of the sandwich structure drastically. Within this paper, a numerical parameter study was carried out to investigate the criticality of initial disbonds in honeycomb sandwich structures under ground-air pressurization. A fracture mechanics approach was used to evaluate the loading at the disbond front. In this case, the strain energy release rate was computed via the Virtual Crack Closure Technique. Special attention was paid to the pressure-deformation coupling which can decrease the pressure load within the disbonded sandwich section significantly when the structure is highly deformed.

15. SUBJECT TERMS

Core disbonding; Crack closure; Finite element; Fracture mechanics; Sandwich structures

16. SECURITY CLASSIFICATION OF:			17. LIMITATION OF ABSTRACT	18. NUMBER OF PAGES	19a. NAME OF RESPONSIBLE PERSON
a. REPORT	b. ABSTRACT	c. THIS PAGE			STI Help Desk (email: help@sti.nasa.gov)
					19b. TELEPHONE NUMBER *(Include area code)*
U	U	U	UU	32	(443) 757-5802